THE JOURNAL OF PHYSICAL CHEMISTRY C

Article

pubs.acs.org/JPCC

Formation of Locally Crystallized Ferroelectric Poly(vinylidene fluoride-*ran*-trifluoroethylene) Nanodots Based on Heated Atomic Force Microscopy

Jong Yeog Son,[†] Inhwa Jung,*[,‡] and Young-Han Shin*[,§]

[†]Department of Applied Physics, College of Applied Science and [‡]Department of Mechanical Engineering, Kyung Hee University, Suwon 446-701, Korea

[§]Department of Physics, University of Ulsan, Ulsan 680-749, Korea

ABSTRACT: We demonstrate locally crystallized ferroelectric poly(vinylidene fluoride-*ran*-trifluoroethylene) (P(VDF-TrFE)) nanodots in a noncrystallized 10 nm thick P(VDF-TrFE) thin film using heated atomic force microscopy (*h*-AFM). Joule heating of the AFM tip made it possible to form crystallized P(VDF-TrFE) nanodots with a size ranging from 40 to 250 nm. Piezoresponse force microscopy was used to characterize the ferroelectric properties of the crystalline P(VDF-TrFE) nanodots. The ferroelectric bit sizes of the P(VDF-TrFE) nanodots were strongly depending on the tip heating bias and time while the ferroelectric bit size of the crystallized ferroelectric P(VDF-TrFE) thin film was directly proportional to the magnitude of the ferroelectric switching bias.

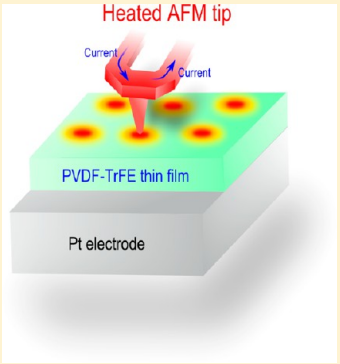

INTRODUCTION

Room-temperature ferroelectric materials with spontaneous polarization and piezoelectricity are useful for nonvolatile random access memory (NVRAM) applications, acoustic sensors, and actuators.[1] A $Pb(Zr,Ti)O_3$ (PZT) ferroelectric field-effect transistor as a NVRAM bit has exhibited a high density along with fast reading and writing speeds at a low operating voltage.[1] Although PZT as a representative ferroelectric material has higher ferroelectric polarization and piezoelectric coefficients than other materials, it contains Pb, which is toxic.[1−3] In terms of environment friendliness, inorganic lead-free oxides such as $BaTiO_3$ and $BiFeO_3$[4−8] or organic ferroelectric copolymers such as poly(vinylidene fluoride-*ran*-trifluoroethylene) (P(VDF-TrFE))[9−19] are promising candidates for the aforementioned applications. In general, nontoxic and flexible ferroelectric polymers have low crystallization temperatures below 200 °C but lower ferroelectric polarization and piezoelectric coefficients than inorganic ferroelectric materials.

Size effects of ferroelectric materials are commonly observed over a wide range from a few micrometers to a few nanometers, which is quite different behavior than nanoscale devices such as quantum dots and nanowires.[1,20−22] For example, the ferroelectric domains of ferroelectric materials exhibit scaling behaviors in ferroelectric polarization and coercive electric fields as a function of size.[1,3,23] In addition, ferroelectric materials have a critical minimum size to maintain its ferroelectricity.[3]

EXPERIMENTAL SECTION

In this study, we show that locally crystallized P(VDF-TrFE) nanodots can be formed in a noncrystallized 10 nm thick P(VDF-TrFE) thin film using a heated atomic force microscope (*h*-AFM). The melting point of P(VDF-TrFE) is >155 °C. Here we chose two annealing temperatures of 160 and 200 °C because the crystallization temperature is ∼140 °C and the bottom electrode of the P(VDF-TrFE) film plays the roll of the heat sink that chills the P(VDF-TrFE) film under the local crystallization process using the *h*-AFM. The P(VDF-TrFE) nanodots exhibit size controllability in the range of 40 to 250 nm as a function of the heating time of the AFM tip. We confirm that the P(VDF-TrFE) nanodots are ferroelectric through piezoresponse force microscopy (PFM) measurements.

P(VDF-TrFE) (70:30 mol % copolymer) films with a thickness of 10 nm were deposited on a (111)-oriented $Pt/TiO_2/SiO_2/Si$ substrate by repeating the Langmuir−Blodgett method 20 times. The Langmuir−Blodgett method has been used to deposit a P(VDF-TrFE) monolayer with a thickness of 0.5 nm onto a substrate by immersing the substrate into a P(VDF-TrFE) solution.[19] AFM and PFM were used to investigate the surface morphology and roughness of the P(VDF-TrFE) films as well as the switching characteristics of the ferroelectric P(VDF-TrFE) nanodots and films, respectively.

RESULTS AND DISCUSSION

Figure 1a shows schematic drawings of the formation of locally crystallized ferroelectric P(VDF-TrFE) nanodots. Before forming the P(VDF-TrFE) nanodots, a noncrystallized P(VDF-TrFE) thin film was annealed for 30 min at 80 °C to solidify the film.

Received: March 25, 2013
Revised: May 29, 2013

   dx.doi.org/10.1021/jp402901g | *J. Phys. Chem. C* XXXX, XXX, XXX−XXX

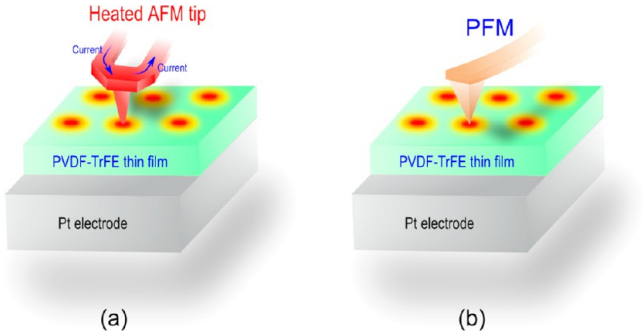

Figure 1. Schematic drawings of the formation of locally crystallized ferroelectric P(VDF-TrFE) nanodots by the *h*-AFM tip. (a) Local heating process using the *h*-AFM tip on a noncrystallized P(VDF-TrFE) thin film. (b) Local surface analysis of locally crystallized ferroelectric P(VDF-TrFE) nanodots in the noncrystallized P(VDF-TrFE) thin film using PFM.

P(VDF-TrFE) nanodots were formed and crystallized under Joule heating of the AFM tip by applying a current through the tip.[24] It is known to be possible to elevate the temperature of the AFM tip to 1000 °C. The surface profile of the film was measured by AFM. The distance between the *h*-AFM tip and the surface was set at 200 nm. When the AFM tip is heated to a temperature between 160 and 200 °C by applying a current through the tip, the AFM tip approaches the surface of the noncrystalline P(VDF-TrFE) film and is located ~5 nm from the surface. Therefore, it does not mechanically damage the surface of the P(VDF-TrFE) film. After applying a local annealing process for a heating time of <10 s, the *h*-AFM tip returns to a distance of 200 nm from the surface. P(VDF-TrFE) nanodots with diameter ranging from 40 to 250 nm are controllable because the dot diameter is a function of the local temperature of the AFM tip as well as the heating time. After formation of crystalline P(VDF-TrFE) nanodots, PFM was

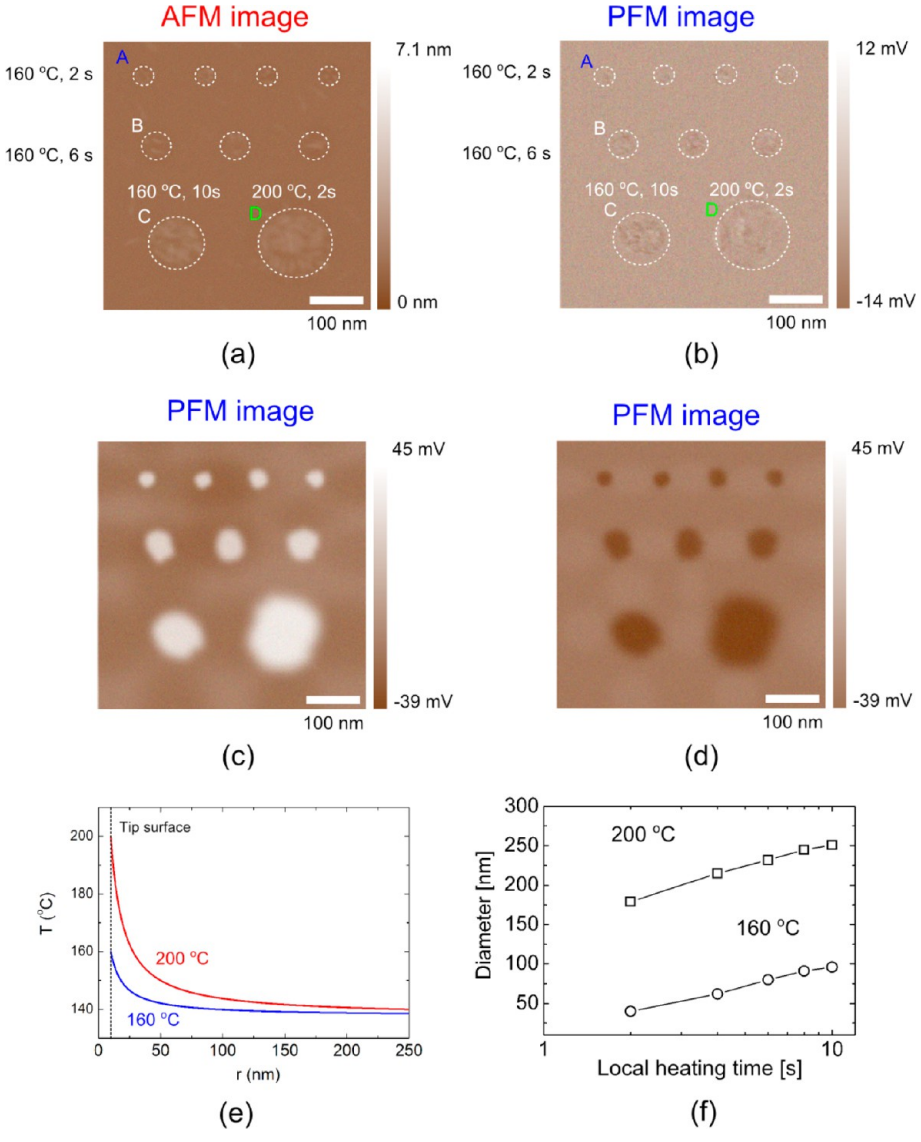

Figure 2. Local surface analysis of the P(VDF-TrFE) nanodot array. (a) AFM image of the P(VDF-TrFE) nanodot array. (b) PFM image of the nanodot after the local annealing process. PFM images of (c) upward and (d) downward polarized nanodot arrays after the switching process. (e) Diameter curves of the P(VDF-TrFE) nanodots as a function of the annealing time for 160 and 200 °C. (f) Calculated steady-state temperature curve as a function of the distance from the AFM tip. The radii of the crystallized boundary of the P(VDF-TrFE) thin film were assumed to be 96 and 251 nm for temperatures of 160 and 200 °C, respectively.

dx.doi.org/10.1021/jp402901g | J. Phys. Chem. C XXXX, XXX, XXX−XXX

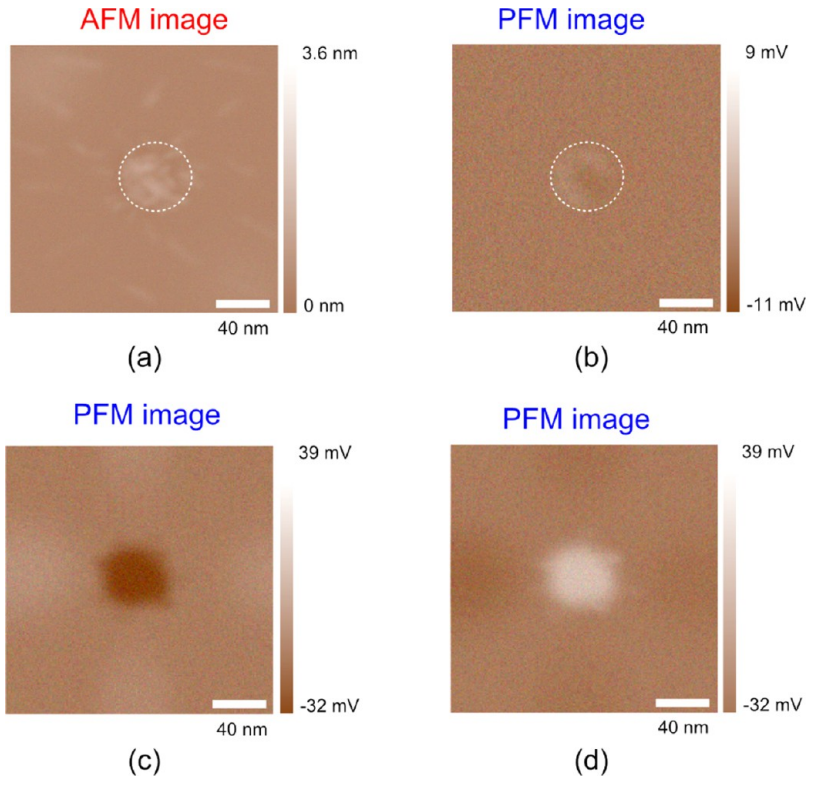

Figure 3. Local surface analysis of the P(VDF-TrFE) nanodot A with a diameter of ~40 nm, as denoted in Figure 2. (a) AFM and (b) PFM images after the local annealing process. PFM images after (c) the upward switching with an applied bias of 5 V and (d) the downward switching with an applied bias of −5 V.

used to study the ferroelectric properties of the crystallized P(VDF-TrFE) nanodots in the noncrystallized P(VDF-TrFE) thin film, as schematically shown in Figure 1b.

Figure 2a,b shows AFM and PFM images of P(VDF-TrFE) nanodots formed by the *h*-AFM tip, respectively, where A, B, C, and D indicate P(VDF-TrFE) nanodots with diameters of 40, 80, 100, and 250 nm, respectively. There are dewetting events in the P(VDF-TrFE) nanodots, in which the thickness of the nanodots slightly increases resulting from the local annealing process. Here the formation conditions of the A, B, C, and D nanodots are 2, 6, and 10 s at 160 °C and 2 s at 200 °C, respectively. All of the P(VDF-TrFE) nanodots are indicated by dotted circles for clarity. The ferroelectric properties of the P(VDF-TrFE) nanodots were confirmed by PFM, as shown in Figure 2b, where domain patterns are observed in all of the P(VDF-TrFE) nanodots.

To confirm the ferroelectric properties, we performed switching processes for the P(VDF-TrFE) nanodots, where the applied biases to the PFM tip for the A, B, C, and D P(VDF-TrFE) nanodots were ±5, ±7, ±10, and ±10 V, respectively, with an applied time of ~1 μs. Here the positive and negative biases were applied to generate downward and upward ferroelectric polarizations, respectively. Figure 2c,d shows PFM images of the P(VDF-TrFE) nanodots with upward and downward ferroelectric polarizations, respectively, where all P(VDF-TrFE) nanodots exhibit single domain structures. The ferroelectric polarizations of all the P(VDF-TrFE) nanodots were well-switched by the applied biases, indicating that all P(VDF-TrFE) nanodots have ferroelectricity. Thus, all of the P(VDF-TrFE) nanodots were well-crystallized by the local annealing process using the *h*-AFM tip. Figure 2e shows the dot diameters of the P(VDF-TrFE) nanodots as a function of the heating time at AFM tip temperatures of 160 and 200 °C. Here it can be seen that the dot diameter is logarithmically proportional to the heating time at each temperature of the AFM tip. To understand the local heating process with the *h*-AFM tip, we calculated the steady-state temperature as a function of the distance from the AFM tip (Figure 2f). Here the AFM tip was assumed to be an ideal hemispherical heat source with a radius of r_0. The crystallized area was also assumed to be a hemisphere with a radius of r_1. The temperatures at the tip and the crystallized boundary of the P(VDF-TrFE) thin film were applied as boundary conditions. A general expression for the temperature distribution can be given by $(T(r) - T(r_1))/(T(r_0) - T(r_1)) = (1 - r_1/r)/(1 - r_1/r_0)$, which is the 1D steady-state solution of the heat equation for a spherical wall.[24,25] The heat equation is expressed as

$$\frac{1}{r^2}\frac{\mathrm{d}}{\mathrm{d}r}\left(r^2\frac{\mathrm{d}T}{\mathrm{d}r}\right) = 0$$

For the calculations, we assumed r_0 to be 10 nm, $T(r_0)$ to be 160 and 200 °C, and r_1 to be 96 and 251 nm at 160 and 200 °C, respectively. For both cases, $T(r_1)$ is assumed to be 140 °C.

Figure 3a shows an AFM image of the P(VDF-TrFE) nanodot with a diameter of 40 nm, where the P(VDF-TrFE) nanodot exhibits grain structures and stripes are located around the P(VDF-TrFE) nanodot. Figure 3b shows a PFM image of the P(VDF-TrFE) nanodot with a diameter of 40 nm, where the P(VDF-TrFE) nanodot exhibits three ferroelectric domains (two upward and one downward ferroelectric polarization) and the stripes observed around the nanodot in the AFM image are not seen. Figure 3c,d shows PFM images of the 40 nm diameter PVDF-TrFE nanodot with upward and downward ferroelectric polarizations, respectively. Notably, the P(VDF-TrFE) nanodot

dx.doi.org/10.1021/jp402901g | J. Phys. Chem. C XXXX, XXX, XXX−XXX

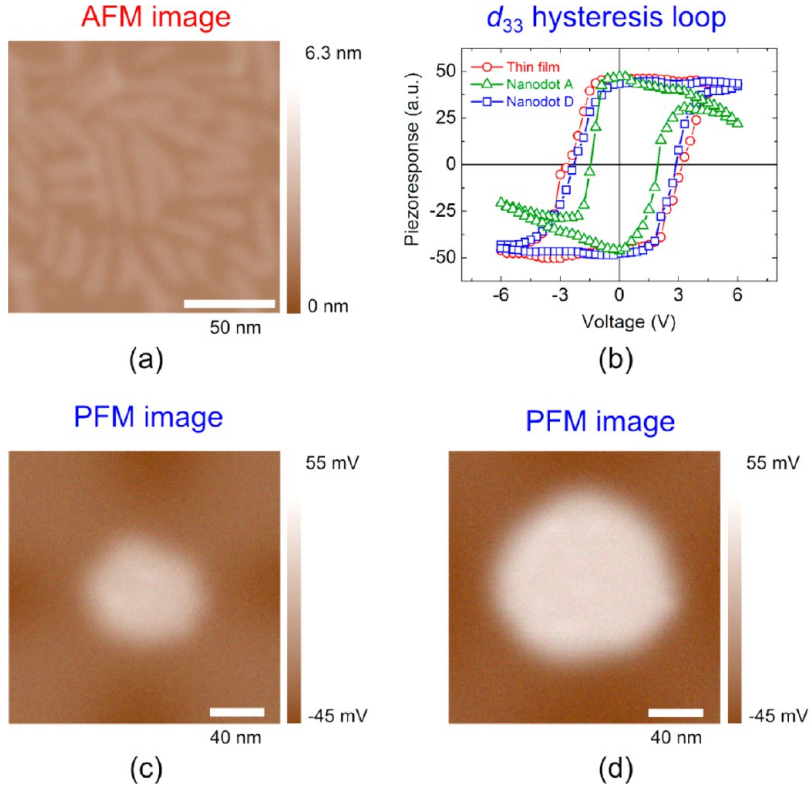

Figure 4. (a) AFM image of the highly crystalline P(VDF-TrFE) thin film. (b) Piezoelectric hysteresis loops of the well-crystallized P(VDF-TrFE) thin film, nanodot A, and nanodot D, as denoted in the AFM image in Figure 2a. PFM images of upward polarization bits in the well-crystallized P(VDF-TrFE) thin films with applied voltages of (c) 5 and (d) 7 V for an applied time of 1 μs.

exhibits a well-defined dot diameter of 40 nm after switching of the ferroelectric polarization because the ferroelectric P(VDF-TrFE) nanodots are well-defined from the noncrystallized P(VDF-TrFE) thin film without ferroelectricity.

To compare the ferroelectric P(VDF-TrFE) nanodot with the ferroelectric P(VDF-TrFE) thin film, a crystallized P(VDF-TrFE) thin film with a thickness of 10 nm was formed by annealing a noncrystallized P(VDF-TrFE) thin film for 40 min at 140 °C. Figure 4a shows an AFM image of the P(VDF-TrFE) thin film where the P(VDF-TrFE) thin film exhibits stripe grains on the surface. Figure 4b shows typical piezoelectric hysteresis loops of the crystallized P(VDF-TrFE) thin film and the two nanodots (nanodot A and nanodot D, as denoted in Figure 2). The coercive voltage of the nanodot D is higher than that of the nanodot A and becomes saturated to the coercive voltage of the thin film as the dot size increases. Figure 4c,d shows PFM image of nanodots formed on the crystalline P(VDF-TrFE) thin film by applying biases of 5 and 7 V to the PFM tip, respectively, where the size of the reversed domain increases as the bias increases. In the case of the nanodot A, however, we could not distinguish the size of the reversed domain at different bias voltages because the size of the crystalline nanodot was already determined at the local annealing process. We suggest that the local heating P(VDF-TrFE) with *h*-AFM can be applied to make a high-density nanobit array, which can be used to store information in NVRAM.

■ CONCLUSIONS

We fabricated size-controllable crystallized P(VDF-TrFE) nanodots with diameters ranging from 40 to 250 nm by locally heating the amorphous P(VDF-TrFE) using the *h*-AFM tip. While the diameter of ferroelectric nanodots is closely related to the heating time and temperature of the *h*-AFM tip, the size of the switchable ferroelectric domain was confined to the crystallized P(VDF-TrFE) nanodot surrounded by the amorphous P(VDF-TrFE). In contrast with the crystallized P(VDF-TrFE) nanodots, the size of the switchable ferroelectric domain in the crystallized P(VDF-TrFE) thin films could be changed depending on the applied bias of the PFM tip and the operation time.

■ AUTHOR INFORMATION

Corresponding Author

*E-mail: ijung@khu.ac.kr (I.J.); hoponpop@ulsan.ac.kr (Y.-H.S.).

Notes

The authors declare no competing financial interest.

■ ACKNOWLEDGMENTS

This work was supported by the National Research Foundation of Korea (NRF) funded by the Ministry of Education, Science and Technology (2011-0027337, 2012R1A2A2A01046451, and 2009-0093818).

■ REFERENCES

(1) Scott, J. F. Applications of Modern Ferroelectrics. *Science* **2007**, *315*, 954−959.
(2) Cohen, R. E. Origin of Ferroelectricity in Perovskite Oxides. *Nature* **1992**, *358*, 136−138.
(3) Junquera, J.; Ghosez, P. Critical Thickness for Ferroelectricity in Perovskite Ultrathin Films. *Nature* **2003**, *422*, 506−509.

(4) Moreau, J.; Michel, C.; Gerson, R.; James, W. Ferroelectric $BiFeO_3$ X-ray and Neutron Diffraction Study. *J. Phys. Chem. Solids* **1971**, *32*, 1315−1320.
(5) Kwei, G. H.; Lawson, A. C.; Billinge, J. L.; Cheong, S.-W. Structure of the Ferroelectric Phases of Barium Titanate. *J. Phys. Chem.* **1993**, *97*, 2368−2377.
(6) Wang, J.; Neaton, J. B.; Zheng, H.; Nagarajan, V.; Ogale, S. B.; Liu, B.; Viehland, D.; Vaithyanathan, V.; Schlom, D. G.; Waghmare, U. V.; et al. Epitaxial $BiFeO_3$ Multiferroic Thin Film Heterostructures. *Science* **2003**, *299*, 1719−1722.
(7) Son, J. Y.; Lee, G.; Jo, M.-H.; Kim, H.; Jang, H. M.; Shin, Y.-H. Heteroepitaxial Ferroelectric $ZnSnO_3$ Thin Film. *J. Am. Chem. Soc.* **2009**, *131*, 8386−8387.
(8) Ryu, S.; Son, J. Y.; Shin, Y.-H.; Jang, H. M.; Scott, J. F. Polarization Switching Characteristics of $BiFeO_3$ Thin Films Epitaxially Grown on Pt/MgO at a Low Temperature. *Appl. Phys. Lett.* **2009**, *95*, 242902.
(9) Kawai, H. The Piezoelectricity of Poly(vinylidene fluoride). *Jap. J. Appl. Phys.* **1969**, *8*, 975−976.
(10) Tashiro, K.; Kobayashi, M. Structural Study of the Ferroelectric Phase Transition of Vinylidene Fluoride-trifluoroethylene Copolymers: 4. Poling Effect on Structure and Phase Transition. *Polymer* **1986**, *27*, 667−676.
(11) Furukawa, T. Ferroelectric Properties of Vinylidene Fluoride Copolymers. *Phase Transitions* **1989**, *18*, 143−211.
(12) Ramer, N. J.; Stiso, K. A. Structure and Born Effective Charge Determination for Planar-Zigzag β-Poly(vinylidene fluoride) Using Density-Functional Theory. *Polymer* **2005**, *46*, 10431−10436.
(13) Fang, F.; Yang, W.; Yang, W. Mechanical Flexible and Electric Fatigue Resistant Behavior of Relaxor Ferroelectric Terpolymer. *J. Appl. Phys.* **2009**, *106*, 034106.
(14) Hu, Z.; Tian, M.; Nysten, B.; Jonas, A. M. Regular Arrays of Highly Ordered Ferroelectric Polymer Nanostructures for Non-Volatile Low-Voltage Memories. *Nat. Mater.* **2009**, *8*, 62−67.
(15) Lee, K. H.; Lee, G.; Lee, K.; Oh, M. S.; Im, S. Flexible Low Voltage Nonvolatile Memory Transistors with Pentacene Channel and Ferroelectric Polymer. *Appl. Phys. Lett.* **2009**, *94*, 093304.
(16) Kusuma, D. Y.; Nguyen, C. A.; Lee, P. S. Enhanced Ferroelectric Switching Characteristics of P(VDF-TrFE) for Organic Memory Devices. *J. Phys. Chem. B* **2010**, *114*, 13289−13293.
(17) Son, J. Y.; Ryu, S.; Park, Y.-C.; Lim, Y.-T.; Shin, Y.-S.; Shin, Y.-H.; Jang, H. M. A Nonvolatile Memory Device Made of a Ferroelectric Polymer Gate Nanodot and a Single-Walled Carbon Nanotube. *ACS Nano* **2010**, *4*, 7315−7320.
(18) Heo, W. J; Kim, W.-J.; Shin, Y.-H.; Lee, E. K. Density Functional Study of α-β Phase Transition of Polyvinylidene Difluoride. *Phys. Status Solidi RRL* **2012**, *6*, 217−219.
(19) Palto, S.; Blinov, L.; Bune, A.; Dubovik, E.; Fridkin, V.; Petukhova, N.; Verkhovskaya, K.; Yudin, S. Ferroelectric Langmuir-Blodgett Films. *Ferroelectrics Lett.* **1995**, *19*, 65−68.
(20) Beenakker, C. W. J. Random-Matrix Theory of Quantum Transport. *Rev. Mod. Phys.* **1997**, *69*, 731.
(21) Wang, C.; Harrington, J.; Preskill, J. Confinement-Higgs Transition in a Disordered Gauge Theory and the Accuracy Threshold for Quantum Memory. *Ann. Phys.* **2003**, *303*, 31−58.
(22) van der Wiel, W. G.; De Franceschi, S.; Elzerman, J. M.; Fujisawa, T.; Tarucha, S.; Kouwenhoven, L. P. Electron Transport through Double Quantum Dots. *Rev. Mod. Phys.* **2002**, *75*, 1.
(23) Catalan, G.; eacute; a, H.; Fusil, S.; Bibes, M.; Paruch, P.; Barth; my, A.; Scott, J. F. Fractal Dimension and Size Scaling of Domains in Thin Films of Multiferroic $BiFeO_3$. *Phys. Rev. Lett.* **2008**, *100*, 027602.
(24) Duvigneau, J.; Schonherr, H.; Vancso, G. J. Nanoscale Thermal AFM of Polymers: Transient Heat Flow Effects. *ACS Nano* **2011**, *4*, 6932−6940.
(25) Incropera, F. P.; Dewitt, D. P. *Fundamentals of Heat and Mass Transfer*; John Wiley & Sons, Inc.: New York, 1990.